Biomechanical Evaluation of Cervical Interbody Fusion Cages for Anterior Cervical Discectomy and Fusion With Variations in Morphology: A Finite Element Analysis

Biomedical Engineering and Computational Biology
Volume 16: 1–10

DOI: 10.1177/11795972251321307

Pechimuthu Susai Manickam[1], Raja Dhason[2], Ryan Bock[3], Sonny Bal[3], Sandipan Roy[1] and Shubhabrata Datta[2]

[1]Centre for Biomechanics, Department of Mechanical Engineering, College of Engineering and Technology, SRM Institute of Science and Technology, Kattankulathur, Tamil Nadu, India. [2]Centre for Composites and Advanced Materials, Department of Mechanical Engineering, College of Engineering and Technology, SRM Institute of Science and Technology, Kattankulathur, Tamil Nadu, India. [3]SINTX Technologies, Salt Lake City, UT, USA.

ABSTRACT: The spinal diseases commonly faced by people in the 19th century included intervertebral disc degeneration, tuberculosis and congenital defects that resulted in neurological impairment and global disability. To address these issues, cervical spine surgery was performed. Modern techniques currently used in spine surgery include interbody devices, pedicle screws, artificial discs and bone grafts. The postoperative complications clinically reported during follow-up include nonunion and implant subsidence, which remain significant drawbacks. The objective of this study is to develop a 3-dimensional finite element model of the C2-C7 cervical spine and validate it against existing experimental studies. The loading conditions considered for this study include a compressive preload of 50 N and a 1 Nm moment applied to the C2 vertebra, with the C7 vertebra fixed at the bottom. In this study, the biomechanical alterations of 4 different cage morphologies were analysed using finite element analysis. Valeo cages with 4 distinct designs were implanted at the C5-C6 level, and physiological motion at the surgical site was studied. Cage subsidence and migration, which can lead to adjacent segment disc degeneration, were also examined. Subsidence was primarily attributed to higher stress encountered in the cage, so stress distribution within the cages was evaluated. Additionally, stress distribution in the anterior plate and screws was analysed. The study concludes that introducing anterior plate and screw fixation helps prevent cage subsidence. Physiological motion at the surgical level was reduced compared to the intact model. Adjacent disc stress was also evaluated and found to be lower than in the intact model.

KEYWORDS: Cage, finite element analysis, cervical spine, ACDF, disc degeneration

RECEIVED: July 2, 2024. **ACCEPTED:** February 2, 2025.

TYPE: Original Research

FUNDING: The author(s) received no financial support for the research, authorship, and/or publication of this article.

DECLARATION OF CONFLICTING INTERESTS: The author(s) declared no potential conflicts of interest with respect to the research, authorship, and/or publication of this article.

CORRESPONDING AUTHOR: Sandipan Roy, Department of Mechanical Engineering, College of Engineering and Technology, SRM Institute of Science and Technology, Potheri, Chengalpattu District, Kattankulathur, Tamil Nadu 603203, India. Emails: sandipan-888roy@gmail.com; sandipag@srmist.edu.in

Introduction

Cervical spine problems include disc degeneration, disc herniation, spondylotic myelopathy and ossification of the ligaments.[1-3] ACDF (Anterior Cervical Discectomy and Fusion) surgery is performed to address these cervical issues.[4] The intervertebral fusion cage and anterior fixation are primarily used in ACDF surgery to maintain stability and restore intervertebral disc height on both the anterior and posterior sides.[5,6] The post-surgical effects of ACDF surgery, such as subsidence, construct failure, misalignment, nonunion or pseudoarthrosis, are attributed to load sharing and stress transfer through the cage and anterior fixation plate.[7,8] ACDF surgery is reported to be the most effective surgical approach for cervical spondylotic myelopathy, particularly in cases with severe intervertebral disc degeneration. Its efficiency is better in terms of cervical spine reconstruction and stabilisation, as well as decompression of the spinal cord caused by disc degeneration. Overall complication rates range from 13.2% to 19.3%. The occurrence of pseudarthrosis in ACDF surgery varies based on the levels of fusion. For single-level fusion, pseudarthrosis rates range from 0% to 4.3%. Readmission rates following ACDF surgery are 5.1% after 1 month and 7.7% after 3 months.[9] The prominence of anterior cervical plates can affect the surrounding tissues, causing postoperative dysphagia and oesophageal injury.[10] Anterior cervical discectomy and fusion is regarded as the best and most effective treatment for cervical myelopathy and radiculopathy.[11,12] Multilevel surgeries present more challenges compared to single-level procedures .[13] In the fusion segment, after fixing the cage, there may be a possibility of abnormal range of motion in the adjacent segments. The abnormal and increased motion in the adjacent level to the fusion segment propagates adjacent segment disc degeneration.[14,15] In ACDF surgery, the commonly used materials are titanium, PEEK, or a combination of both, which may provide better properties.[16] The cages currently available come in various shapes and sizes. The shapes of the cages include trapezoidal, rectangular and wedge-shaped designs.[17-19] The morphology of the cage plays a crucial role in the fusion process. Bone growth determines the success rate of fusion. Researchers have conducted studies on cervical cages that may be used for ACDF surgery.

Silicon nitride is an effective bio-ceramic material. Its toughness and strength make it a desired biomaterial for the implant.[20] The silicon nitride is found as a best biomaterial

because it provides good toughness and the strength as an implant. The major advantage of Si_3N_4 is that it provides better osteoconductivity,[21-23] bacteriostasis and lack of subsidence of the cage in the cervical spine.[24] It improves radiolucency, wear resistance,[25] and supports the spinal fusion of the cage with the vertebra. This bioceramic material enhances the structural stability and bioactivity of the implant.[26,27] The metallic biomaterials used in implant design include cobalt-chromium alloys and titanium, while the biopolymers include UHMWPE and PEEK. Silicon nitride exhibits higher compressive strength compared to other biomaterials.[28,29] Its fracture toughness is greater than that of oxide bioceramics.[30] Additionally, silicon nitride has a low coefficient of friction and superior wear resistance.[31] Compared to metal implants, it provides better imaging properties with MRI or CT techniques.[32]

When compared to titanium and PEEK as implant materials, silicon nitride promotes an environment conducive to bone tissue healing. However, its major disadvantages include low energy dissipation and higher manufacturing costs.[20] Currently, silicon nitride is used in implant devices for the cervical and lumbar spine.

Finite element analysis is an effective tool that provides valuable insights in biomechanical studies. It allows the investigation of scenarios impractical for human clinical studies. For example, it can evaluate intradiscal stress in the implant after cage placement and the range of motion in individual functional spine units.

In existing interbody fusion cages, common issues include subsidence of the fusion cages into adjacent vertebrae, adjacent segment intervertebral disc degeneration, and migration of the fusion cage.

This study aims to evaluate the biomechanical alterations following the placement of 4 different interbody fusion cages in the cervical spine at the C5-C6 level. The primary objectives are to:

1. Establish a finite element model of the cervical spine from the C2-C7 levels and simulate the model with different cage geometries at the C5-C6 level.
2. Compare the stress distribution in the cages and the anterior plate with screws for all physiological motions.
3. Analyse the adjacent disc stress for each cage.
4. Measure the subsidence of the cage for all geometries.

Materials and Methods

Intact FE model

An intact model of the cervical spine from C2 to C7 was generated using image processing software, based on a subject considered to be a 35-year-old male. The images were imported into Mimics 10.01 (Materialise Inc., Leuven, Belgium) for the reconstruction of the vertebrae. The thresholding option was used to differentiate the soft tissues from bone. After region-growing, the irregular surfaces were modified without compromising the geometry.

The geometry of the vertebrae was then exported to reverse engineering software, Geomagic DesignX16.0 (Geomagic Inc., North Carolina, USA), for smoothing operations. The irregular solid model was converted into a surface model using Geomagic's smoothing functions. The meshing of the vertebrae, intervertebral discs and ligaments was performed using HyperMesh-21® software (HyperMesh, Altair Engineering®, USA). Element types and material properties were assigned as part of the preprocessing for the finite element model. The meshing of the surface model was completed in HyperMesh.

The anterior and posterior sides of the vertebrae were separated. The intervertebral disc was divided into the annulus fibrosus and nucleus pulposus, and the disc was covered with vertebral endplates on both the anterior and posterior sides.

The implant was designed using SolidWorks. Anterior plates and screws were modelled, with 4 screws inserted into the C5 and C6 vertebrae. At the surgical level (C5-C6), a cage was inserted. The surface and finite element model are shown in Figure 1.

Design of cage with anterior fixation for C5-C6 level and finite element modelling

At the C5-C6 level, the first cage model, Valeo II C, has a length of 14 mm, a width of 12 mm and a convex height of 6 mm. It is named Valeo M-1 and was inserted into the surface model. The second cage model considered, also Valeo II C, has a length of 14 mm, a width of 12 mm and a height of 8 mm. It is named Valeo M-2.

The third cage model, Valeo II C, has a length of 16 mm, a width of 14 mm and a convex height of 6 mm. It is named Valeo M-3. The fourth cage model, Valeo II C, has a length of 16 mm, a width of 14 mm and a height of 8 mm. It is named Valeo M-4.

For all 4 models, an anterior plate and screws were inserted. The individual dimensions are provided in Table 1. The anterior and posterior heights of the plate are also mentioned in Table 1, as shown in Figure 2. The geometry of the plates and screw with dimensions were provided as Supplemental Materials.

The cervical spine finite element model in this study includes the C2 to C7 vertebral bodies, posterior structures, intervertebral discs, vertebral endplates and 5 major ligaments. The cage was inserted at the C5-C6 level. The vertebrae, intervertebral discs, and cage were modelled using first-order solid tetrahedral elements. The interaction between the cage and vertebra was defined as frictional surface-to-surface contact with a coefficient of friction of 0.3.[33,34] The geometrical model of the intervertebral disc was modelled using Pooni et al.[35] The annulus and the nucleus were modelled as separate entities and the material properties assigned were shown in the Table 2. The interaction between the bone graft and the cage was defined as surface-to-surface contact with a coefficient of friction of 0.07.[36] The ligaments used in this study include the anterior longitudinal ligament (ALL), capsular ligament (CL),

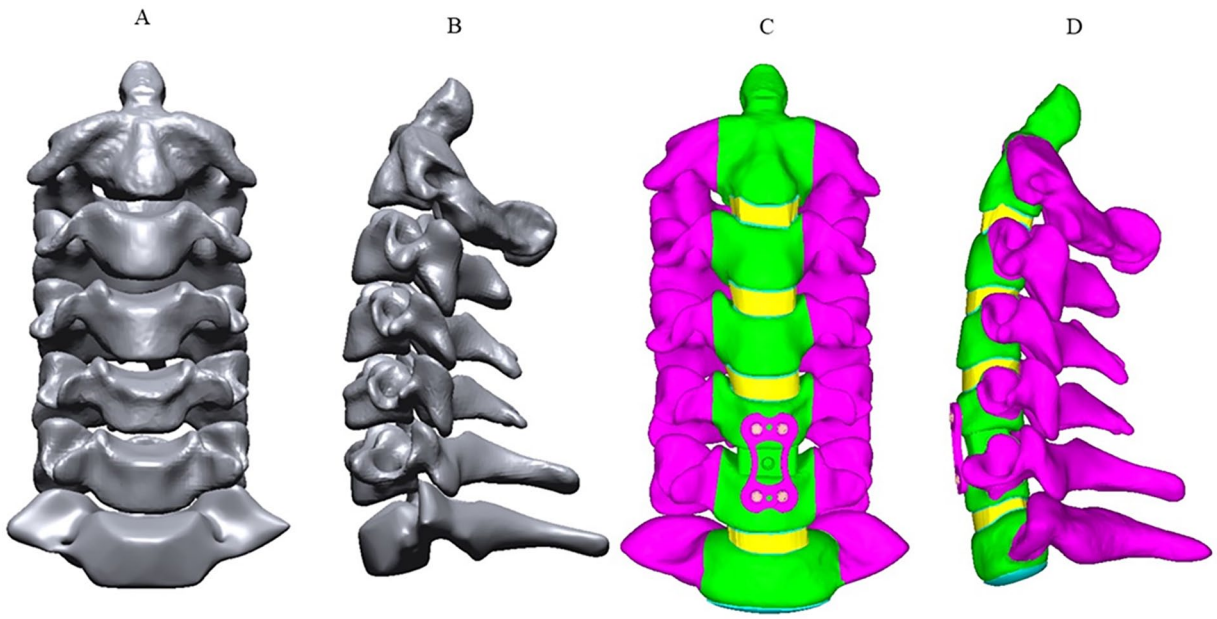

Figure 1. Surface model Intact cervical spine C2-C7 and cage implant model, (A) frontal view of the intact cervical spine, (B) lateral view of the intact cervical spine, (C) frontal view of C2-C7 with implant at C5-C6 level and (D) lateral view of C2-C7 with implant at C5-C6.

Table 1. Dimensions of the Valeo cage with dimensions.

MODEL	DIMENSIONS	ANTERIOR HEIGHT A_H (IN MM)	POSTERIOR HEIGHT P_H (IN MM)	CONVEX (IN MM)	TAPER (IN DEGREES)
Valeo M-1	Valeo II C 14 × 12 Convex 6 mm	9	8	6	-
Valeo M-2	Valeo II C 14 × 12 8 mm	9	8	6	-
Valeo M-3	Valeo II C 16 × 14 Convex 6 mm	10	8	-	6
Valeo M-4	Valeo II C 16 × 14 6 8 mm	10	8	-	6

posterior longitudinal ligament (PLL), ligamentum flavum (LF) and interspinous ligament (ISL). The geometry of the ligaments was constructed based on values from the literature,[37] and they were modelled using tension-only link elements.

In the surgical simulation, the anterior longitudinal ligament and the intervertebral disc were completely removed at the C5-C6 level. The components were divided to assign material properties, as shown in Table 2. The cage material was assigned as silicon nitride, while the anterior fixation components were modelled using titanium plates and screws.[38-40]

Following a convergence test, it was determined that a 0.5 mm element size was optimal.[41] The accuracy of the convergence test for the finite element model was found to be 3%.[41] The meshed model of the cages is shown in Figure 2.

Loading and boundary condition

The meshed model was imported into ANSYS 18.2 (ANSYS, Inc., USA). The 6 physiological motions in this study were simulated using 6 loading conditions of the cervical spine. The finite element model was validated against both experimental and finite element studies.[42]

A compressive load of 50 N was applied to the C2 vertebra, along with a 1 Nm moment in the sagittal, axial and frontal planes to simulate flexion, extension, left lateral bending, right lateral bending, left axial rotation, and right axial rotation.[43,44] The nodes on the inferior surface of the C7 vertebra were constrained.

Results

Range of motion

The intersegmental motion was analysed for all levels of the cervical spine following the placement of the cage at the C5-C6 level. At the C2-C3 level, the range of motion was studied and compared with the intact model. It was observed that with the Valeo M-1 and Valeo M-2 cages, the motion was reduced by 17.4% and 21.7%, respectively, during left axial rotation. For the Valeo M-3 cage, motion during right lateral bending was reduced by 16.1%, and for the Valeo M-4 cage, motion during right axial rotation decreased by 20.8%. At the C3-C4 level,

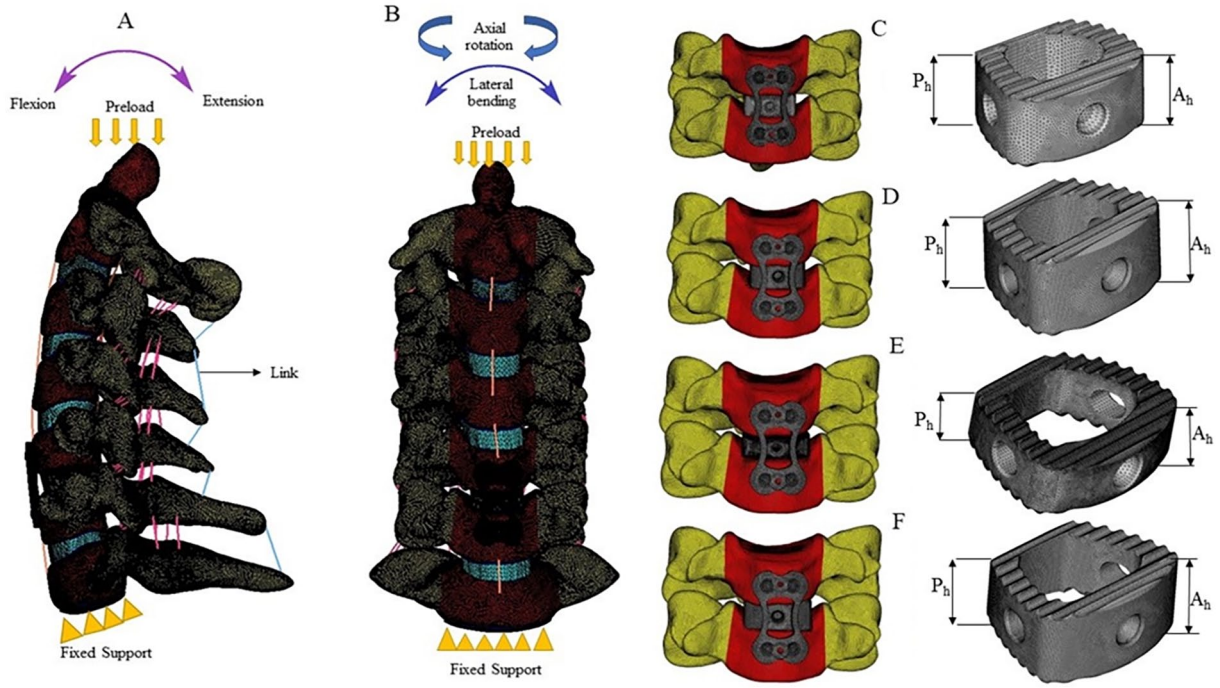

Figure 2. Meshed model: (A) frontal view of C2-C7 with implant at C5- C6 level, (B) lateral view of C2-C7 with implant at C5-C6, (C) Valeo M-1 cage at C5-C6 level, (D) Valeo M-2 cage at C5-C6 level, (E) Valeo M-3 cage at C5-C6 level and (F) Valeo M-4 cage at C5-C6 level.

Table 2. Material properties and element details of components of the developed FE model.

COMPONENT	ELEMENT TYPE	YOUNG'S MODULUS (MPA)	POISSON'S RATIO	CROSS-SECTIONAL AREA (MM^2)	REF
Bony structures					Zhang et al[38]
Cortical bone	Tetrahedral	12000	0.29		Zhang et al[38]
Cancellous bone	Tetrahedral	450	0.29		Zhang et al[38]
Posterior bone	Tetrahedral	3500	0.29		Zhang et al[38]
End plate	Tetrahedral	500	0.4		Zhang et al[38]
Intervertebral disc					Zhang et al[38]
Annulus fibrosus	Tetrahedral	3.4	0.4		Zhang et al[38]
Nucleus pulposus	Tetrahedral	1	0.49		Zhang et al[38]
Ligaments					
ALL	Link (Tension Only)	30		6	Zhang et al[38,39]
PLL	Link (Tension Only)	20		5	Zhang et al[38,39]
ISL	Link (Tension Only)	1.5		10	Zhang et al[38,39]
LF	Link (Tension Only)	1.5		10	Zhang et al[38,39]
CL	Link (Tension Only)	20		5	Zhang et al[38,39]
Implant					
Titanium plate and screw	Tetrahedral	110000	0.3		Wu et al[33]
Silicon nitride	Tetrahedral	297000	0.3		Arab et al[41]

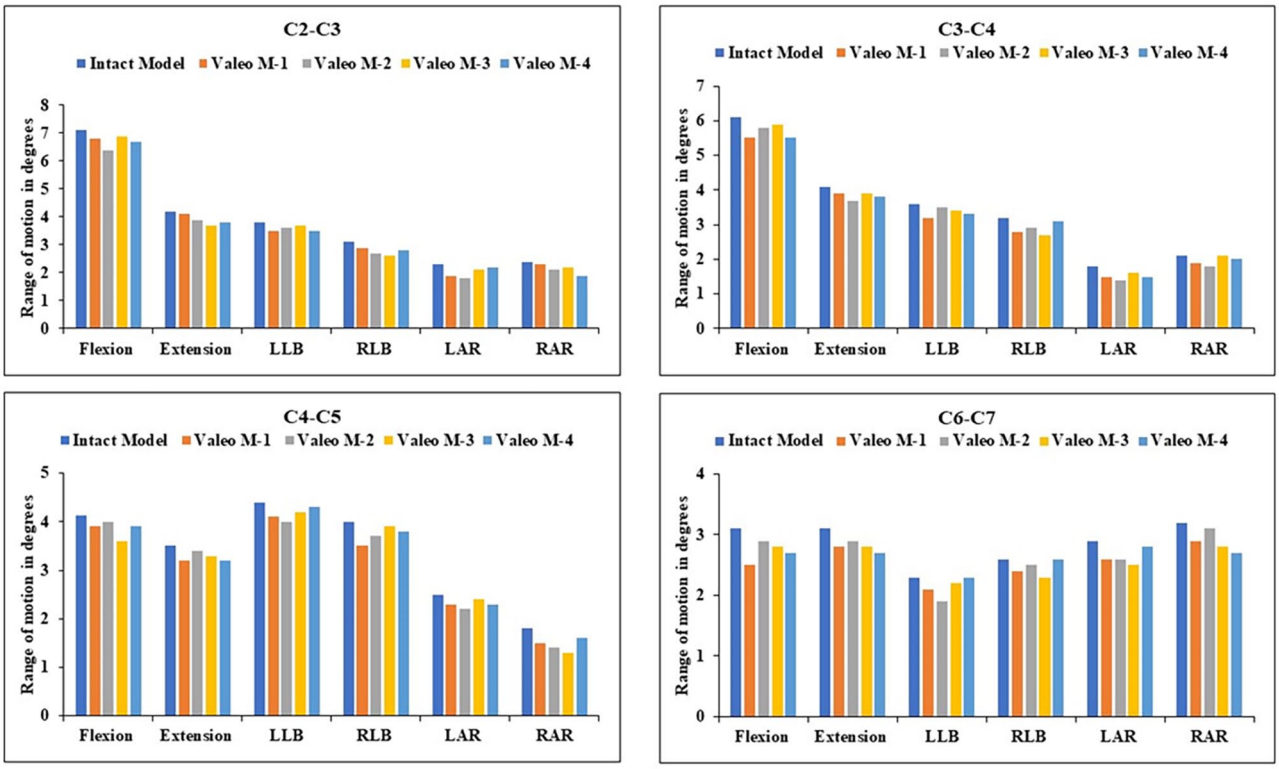

Figure 3. Comparison of range of motion for Valeo M-1 cage, Valeo M-2 cage, Valeo M-3 cage and Valeo M-4 cage with the intact model.

the range of motion was also compared with the intact model. The Valeo M-1 and Valeo M-2 cages reduced motion by 16.7% and 22.2%, respectively, during left axial rotation. For the Valeo M-3 cage, motion during right lateral bending was reduced by 15.6%, while for the Valeo M-4 cage, motion during left axial rotation decreased by 16.7%.

At the C4-C5 level, motion during right axial rotation was reduced by a maximum of 27.8% across all models. At the C6-C7 level, for the Valeo M-1 cage, motion during flexion was reduced by 19.4%. For the Valeo M-2 cage, motion during left lateral bending was reduced by 17.4%. For the Valeo M-3 cage, motion during left axial rotation was reduced by 13.8%, and for the Valeo M-4 cage, motion during right axial rotation decreased by 15.6%. In summary, across all levels, motion was reduced for all physiological motions in comparison with the intact model. The physiological motion for the 4 cages was compared with the intact model, as shown in Figure 3.

Range of motion in the surgical level C5-C6

In the cage fixed level C5-C6 the motion was analysed in that the left lateral bending the motion was reduced by 56% for the Valeo M-1 cage. In the left axial rotation, the Valeo M-2 cage, the motion was reduced by 54.5%. In the Valeo M-3 cage in the right lateral bending the motion was reduced by 57.1%. In the Valeo M-4 cage in flexion motion was reduced by 60%. The surgical level range of motion is shown in Figure 4.

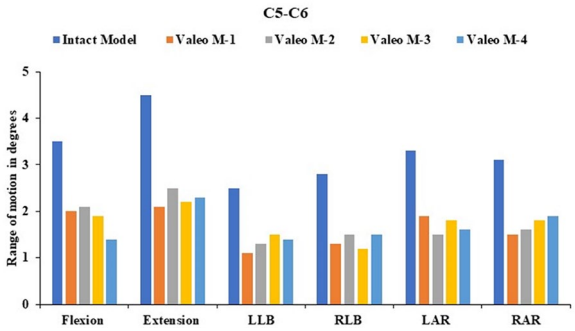

Figure 4. Surgical level range of motion compared with intact model.

Stress analysis for the Valeo cage

The stress analysis of the cage was analysed for the Valeo M-1 in the left lateral bending the stress is around 650.4 MPa and in the flexion the stress was 120.8 MPa and it is less when compared with the other physiological motion. For the Valeo M-2 in the left lateral bending the stress is around 830.4 MPa and in the flexion the stress was 95.5 MPa and it is less when compared with the other physiological motion. For the Valeo M-3 in the right lateral bending the stress is around 1853.9 MPa and in the flexion the stress was 293.2 MPa and it is less when compared with the other physiological motion. For the Valeo M-4 in the right lateral bending the stress is around 724.8 MPa and in the flexion the stress was 119.9 MPa and it is less when compared with the other physiological motion. The stress analysis in the cage is shown in the Figure 5. The average stress values of the cages were given in the Figure 6.

Stress analysis in the anterior fixation

The stress analysis for the anterior fixation was analysed for all the cage models; the stress was varied from 577.1 for the Valeo M-2 model and 336.5 for the Valeo M-4 model in extension motion. The lesser stress values were seen for flexion in the Valeo M1, M3 and M4 and its stress is around 100.4, 85 and 70.87 MPa. In the left axial rotation for the Valeo-M2 the stress is 177.8 MPa. The stress analysis in the anterior fixation is shown in Figure 7. The average stress values of the anterior fixation with screws are given in Figure 8.

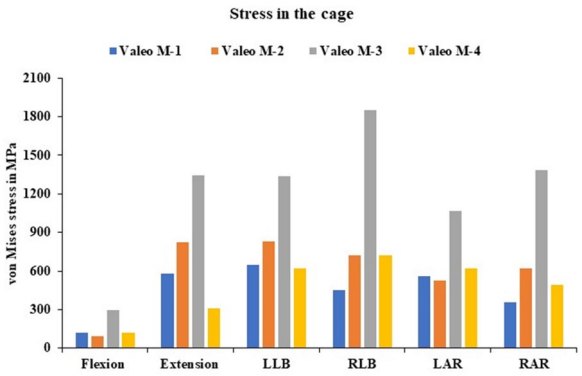

Figure 5. von Mises stress values in the cage for Valeo M-1 cage, Valeo M-2 cage, Valeo M-3 cage and Valeo M-4 cage.

Adjacent side disc stress analysis

The intervertebral disc stress in the superior adjacent disc C4-C5 level were studied in all the cages. We found similar results: the stress values were reduced varied from 79.7% to 71% during the flexion motion when compared with the intact model. In the inferior adjacent segments C5-C6 level, we observed the stress values are higher for all the cage and it varied from 49% to 154% during the left axial rotation; the values look higher when we compare with the intact model. The adjacent side intradiscal pressure is shown in Figure 9.

Subsidence of the interbody cage

The subsidence was studied for all the physiological motion for the different geometry cages. The Valeo M-1 cage subsidence was 0.3 mm during extension which is a higher value and 0.1 mm during the axial rotation. The Valeo M-2 cage subsidence was 0.3 mm during flexion, right lateral bending and left axial rotation and 0.1 mm during left lateral bending. The Valeo M-3 cage subsidence was 0.4 mm during extension and

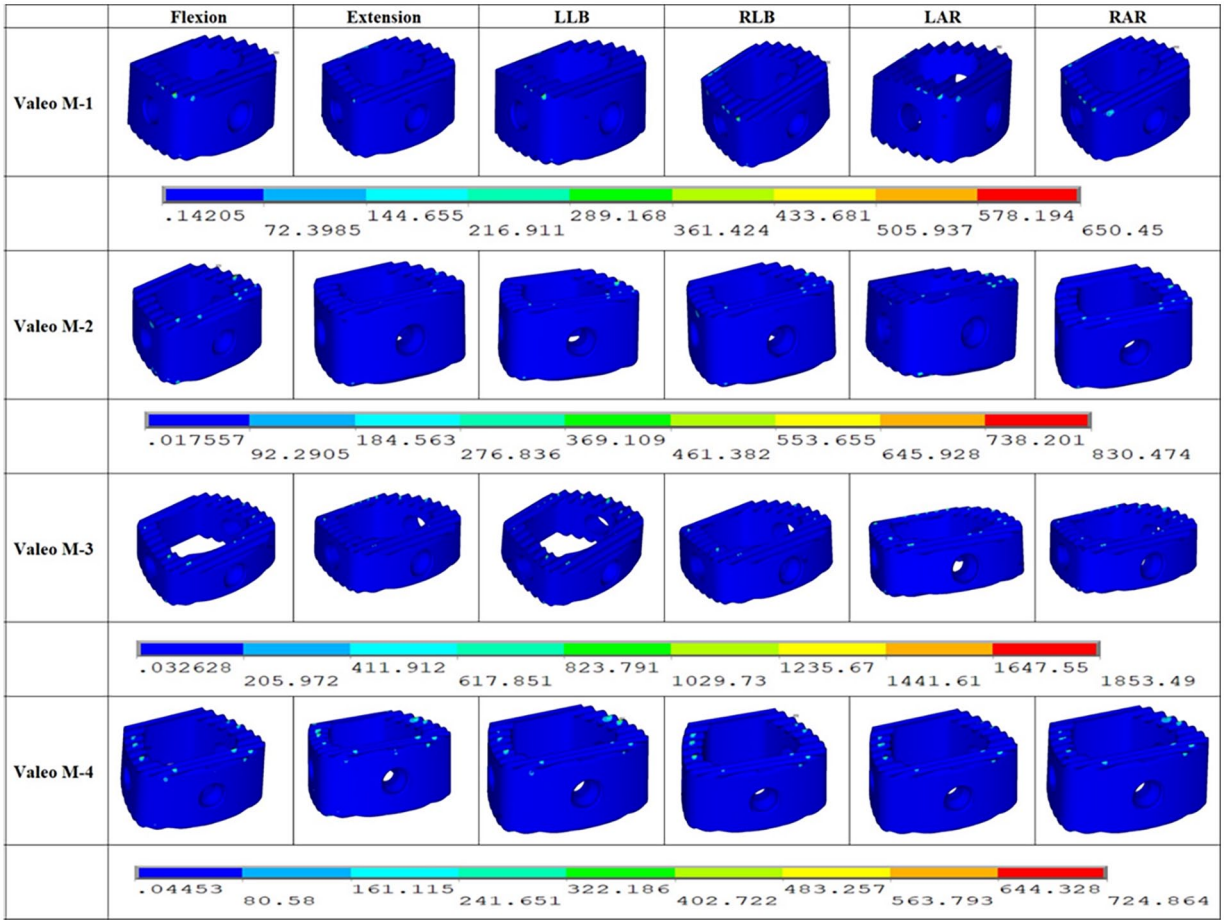

Figure 6. von Mises stress in the Valeo cage.

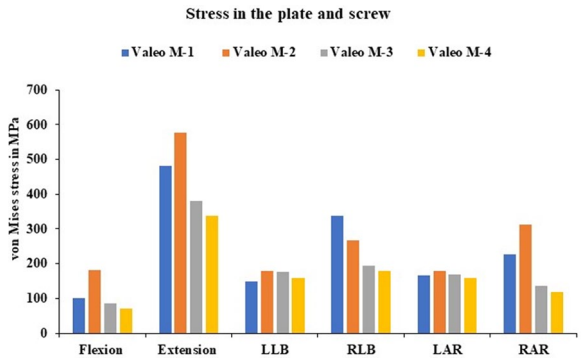

Figure 7. von Mises stress values in the plate and screw for Valeo M-1 cage, Valeo M-2 cage, Valeo M-3 cage and Valeo M-4 cage.

0.1 mm during flexion. The Valeo M-4 cage subsidence was 0.4 mm during extension and 0.1 mm during left lateral bending, right axial rotation. The subsidence of the cage is shown in Figure 10.

Discussion

The author Igarashi et al , studied the age at which the cage subsidence will occur in that they took 78 patients, the age was from 30 to 79 years, and in the results, they found there is no correlation between the age of the patient and the cage subsidence.[45] In a retrospective study, age groups of 18 to 70 were considered in that there is no significant correlation between the patient age and the subsidence of the cage. Hamada and Abou-Zeid.[46,47] Nakanishi et al,[48] in this study, considered 42 patients and found there is no relation between the cage subsidence and the age of the patients. Bone mineral density between the end plate and the vertebral body plays a major role in the estimation of the intervertebral cage subsidence. Jin et al[49] and Lim et al[50] proposed that mechanical loads, when compared to the thickness of the vertebral endplate, cause failure. From this analysis we found the bone mineral density is inversely proportional to the interbody fusion cage subsidence.[51,52] These finite element simulation findings demonstrate the influence of the material composition and the geometry of the cage for the cervical spine. A s-type dynamic cage was developed with titanium and PEEK material to find the best shape of the cage with bone graft because a higher stress in the cage will cause subsidence.[53,54] In the ACDF surgery, after the cage is fixed between the vertebrae, a micromotion may exist between the vertebrae, and due to that the fusion rate may be failed so in order to control the motion and promote the fusion rate it is necessary to provide anterior fixation screw and plate system. In the recent studies it was reported that after the anterior plate fixation will promote a higher fusion rate.[55,56] Bartels et al[57] demonstrated that the incidence of the cage subsidence is higher in the C6-C7 level when we compared with the other fusion level. Barsa and Suchomel[56] et al reported that in the superior level the contact area is high when compared with the inferior level contact area so due to lower contact are may cause subsidence of the cage. Yang et al[58] also reported the smaller diameter of the cage will impact a higher subsidence of the cage. Recent studies reveal that cage subsidence, a major complication after ACDF surgery, manifests in both the postoperative and final follow-up periods. The factors involved were the intervertebral nonunion of the cage, adjacent segment disc degeneration and loss of the lordosis.[58]

Ceramic materials are known for their strength and durability. Also, it has distinct failure characteristics. The Weibull modulus assesses the diversity in strength, with higher values implying a lower risk of failure. Additionally, factors such as microstructure, loading rate, temperature, and environment significantly influence the risk of ceramic failure. Apart from flexural and compressive strength, fracture toughness is also an important part of the materials.

Due to localised deformation, the growth of cracks propagates as a key failure as an antisymmetric mode before evolving into symmetric patterns. Furthermore, residual stress within the material can intensify the failures. The failure starts with surface exfoliation, where layers of material peel off.

Under compression and high temperatures, the characteristics of silicon nitride need to be investigated for thermal and mechanical stability because of its long-term reliability in high-stress environments.[59]

The range of motion across the surgical level C5-C6 was studied, and the results show that in all 4 cages, it exhibited less motion when compared with the intact model.[60] The stress distribution in the cage was studied in that we found a higher stress is seen in the Valeo M-3 model in all the physiological motion. Whereas in flexion the cage exhibits much less stress when compared with all the other physiological motion. The stress distribution in the anterior plate and the screw was studied in that we found in extension motion the stress was higher for all the cages. The major problem after the cage implant is the increase of the adjacent segment disc degeneration due to the restricted mobility in the surgical level and the hypermobility in the adjacent level. Therefore, we conducted a study on the stress in the adjacent segment disc after the cage was implanted. In the C4-C5 superior adjacent level, we observed a higher stress in both the left and right axial rotation. In the C6-C7 level the inferior adjacent segment disc stress was higher in the left axial rotation. In all the other physiological motion the intervertebral disc stress is less when compared with the intact model. The subsidence is the very important factor which leads to the cage dislocation migration and cage sinking. In all 4 cages we found the micromotion, which is less than 0.5 mm. So, the cage subsidence is very less in the cages. In all the cages initially, the subsidence was high, so we introduced anterior fixation with screws to prevent the subsidence in the interbody fusion cage.

The limitation of this study is that we assumed a simplified model, and the material property for the FE model was modelled as linear isotropic elements. The fibres in the annulus fibrosus were not considered in our study.

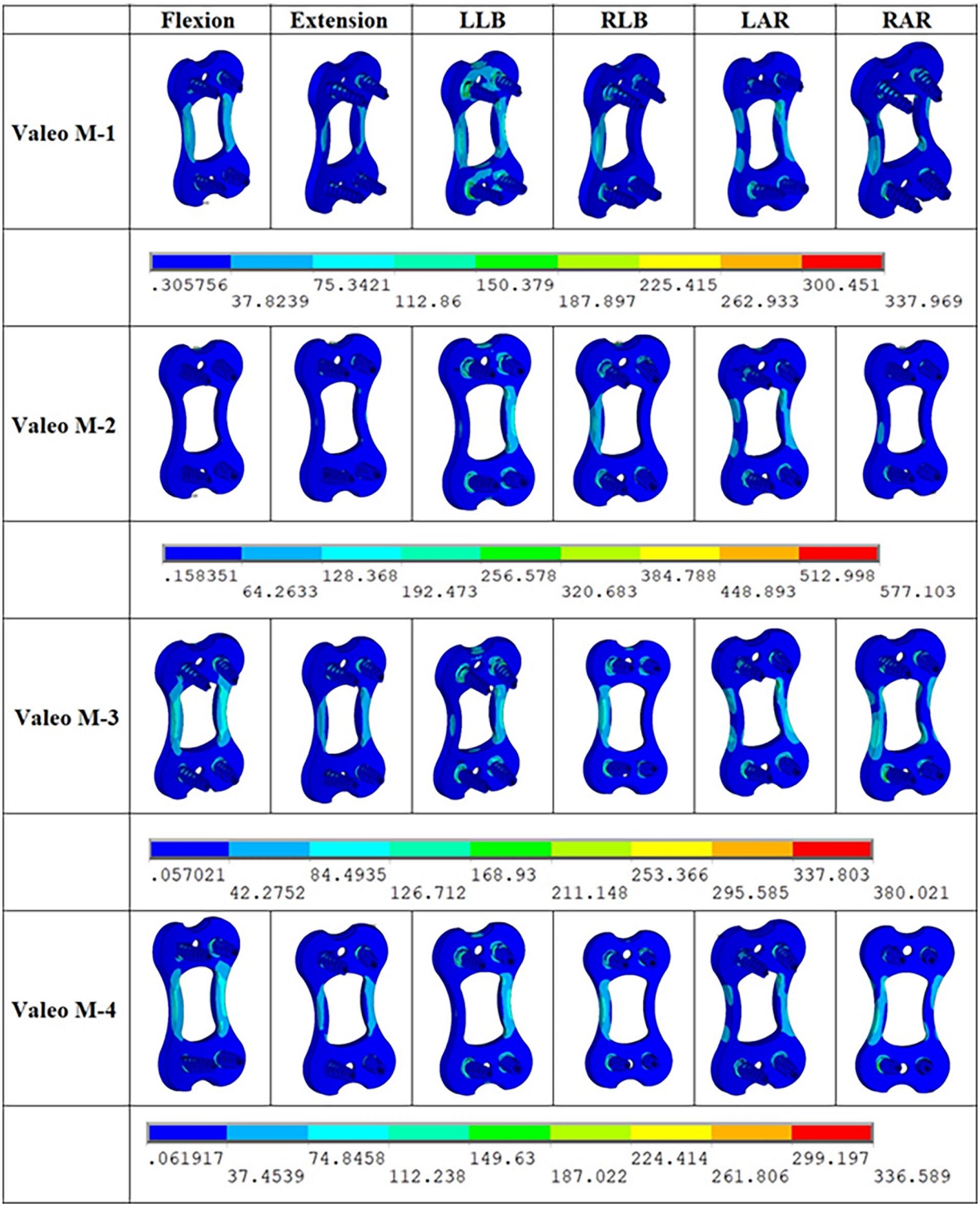

Figure 8. von Mises stress in the anterior plate and the screw.

Conclusion

The finite element study is conducted to evaluate the biomechanical alteration of the 4 different design Valeo cages during ACDF surgery. In the present study, the 4 differently designed fusion cages were selected, and the concept of the design was studied. The factors that are studied here are the physiological motion at the surgical level in that we found the motion is much less when compared with the intact model. The stress distribution across the cage was studied for all the 4 different constructs. The subsidence in the cage was studied, and we found in all the models it is less than 0.5 mm. We confirmed it will not allow the cage to sink or migrate because of this micromotion. The adjacent side disc stress was also studied, and we found it is less when compared with the intact model, so here we confirmed that after the implantation of the cage, there will not be any adjacent segment disc degeneration. The variously

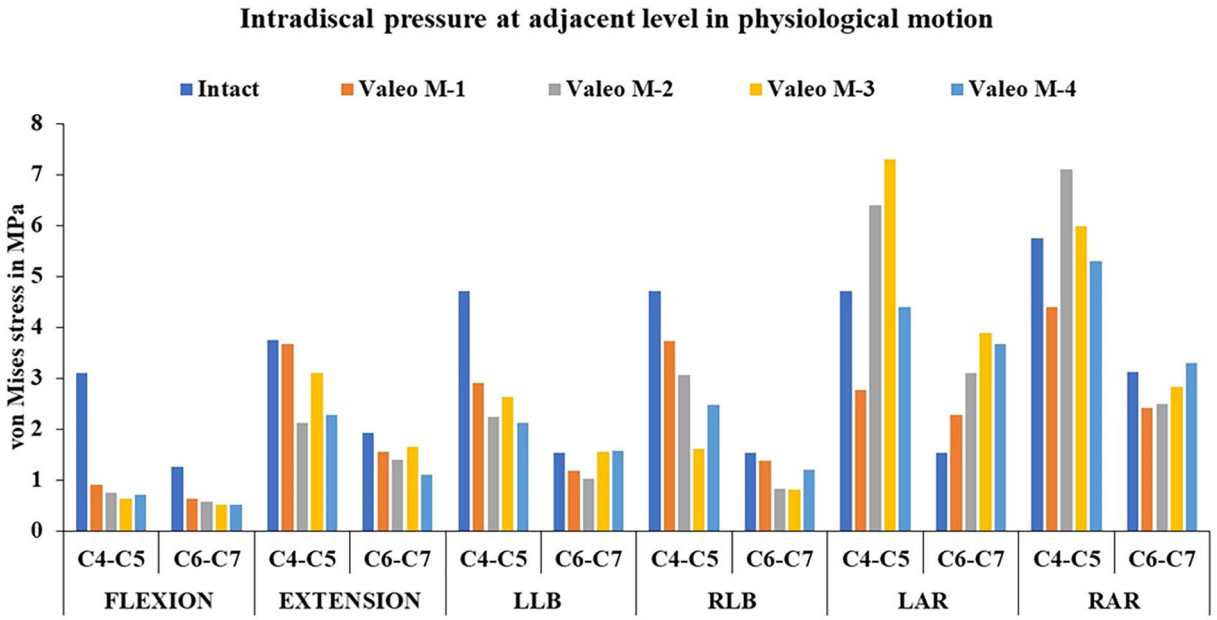

Figure 9. Intradiscal stress at adjacent segments C4-C5 and C6-C7 level.

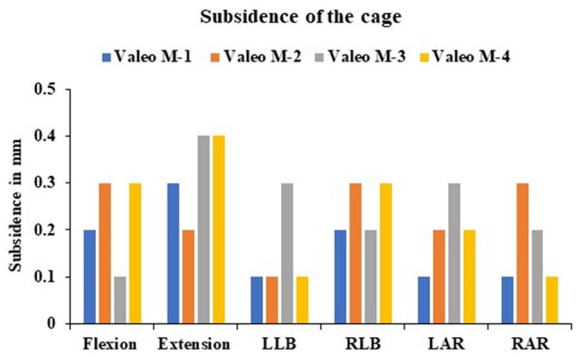

Figure 10. Subsidence in the cage at the C5-C6 level.

designed cages may exhibit different biomechanical behaviour in the human cervical spine after the ACDF surgery. In this work the authors are doing a framework using finite element study and finding the best design that reduces the subsidence of the cage. This will help the surgeon's community to choose the appropriate design for the patients.

Author Contributions

Conceptualization: RB, SB; Methodology: PSM, RD; Software: PSM; Writing – Original Draft: PSM; Writing – Review & Editing: PSM, SR; Supervision: RB, SB SR, SD; Funding acquisition: RB, SB.

ORCID iDs

Pechimuthu Susai Manickam https://orcid.org/0000-0001-7507-5726

Raja Dhason https://orcid.org/0000-0001-6912-697X

Sandipan Roy https://orcid.org/0000-0002-6888-272X

Shubhabrata Datta https://orcid.org/0000-0002-7716-9205

Supplemental material

Supplemental material for this article is available online.

REFERENCES

1. Inoue N, Espinoza Orías AA. Biomechanics of intervertebral disk degeneration. *Orthop Clin North Am*. 2011;42:487-499.
2. Adams MA, Dolan P, McNally DS. The internal mechanical functioning of intervertebral discs and articular cartilage, and its relevance to matrix biology. *Matrix Biol*. 2009;28:384-389.
3. Tao Y, Galbusera F, Niemeyer F, et al. Radiographic cervical spine degenerative findings: a study on a large population from age 18 to 97 years. *Eur Spine J*. 2021;30:431-443.
4. Cloward RB. The anterior approach for removal of ruptured cervical disks. *J Neurosurg*. 1958;15:496-617.
5. Kapetanakis S, Thomaidis T, Charitoudis G, et al. Single anterior cervical discectomy and fusion (ACDF) using self-locking stand-alone polyetheretherketone (PEEK) cage: evaluation of pain and health-related quality of life. *J Spine Surg*. 2017;3:312-322.
6. Prusick PJ, Sabri SA, Kleck CJ. Expectoration of anterior cervical discectomy and fusion cage: a case report. *J Spine Surg*. 2021;7:218-224.
7. Zhang L, Wang J, Feng X, et al. Outcome evaluation of zero-profile device used for single-level anterior cervical discectomy and fusion with osteoporosis compared without osteoporosis: a minimum three-year follow-up study. *World Neurosurg*. 2019;124:e1-e9.
8. Kao TH, Wu CH, Chou YC, et al. Risk factors for subsidence in anterior cervical fusion with stand-alone polyetheretherketone (PEEK) cages: a review of 82 cases and 182 levels. *Arch Orthop Trauma Surg*. 2014;134:1343-1351.
9. Epstein NE. A review of complication rates for anterior cervical diskectomy and fusion (ACDF). *Surg Neurol Int*. 2019;10:100-108.
10. Park JB, Cho YS, Riew KD. Development of adjacent-level ossification in patients with an anterior cervical plate. *J Bone Joint Surg*. 2005;87:558-563.
11. Fehlings MG, Wilson JR, Kopjar B, et al. Efficacy and safety of surgical decompression in patients with cervical spondylotic myelopathy: results of the AOSpine North America prospective multi-center study. *J Bone Joint Surg*. 2013;95:1651-1658.
12. Wang B, Liu H, Wang H, Zhou D. Segmental instability in cervical spondylotic myelopathy with severe disc degeneration. *Spine*. 2006;31:1327-1331.
13. Eck JC, Humphreys SC, Lim TH, et al. Biomechanical study on the effect of cervical spine fusion on adjacent-level intradiscal pressure and segmental motion. *Spine*. 2002;27:2431-2434.
14. Hilibrand AS, Carlson GD, Palumbo MA, Jones PK, Bohlman HH. Radiculopathy and myelopathy at segments adjacent to the site of a previous anterior cervical arthrodesis. *J Bone Joint Surg*. 1999;81:519-528.

15. Saavedra-Pozo FM, Deusdara RA, Benzel EC. Adjacent segment disease perspective and review of the literature. *Ochsner Journal*. 2014;14:78-83.
16. Li ZJ, Wang Y, Xu GJ, Tian P. Is PEEK cage better than titanium cage in anterior cervical discectomy and fusion surgery? A meta-analysis. *BMC Musculoskelet Disord*. 2016;17:1-9.
17. Manickam PS, Roy S. The biomechanical effects of S-type dynamic cage using Ti and PEEK for ACDF surgery on cervical spine varying loads. *Int J Artif Organs*. 2021;44:748-755.
18. Manickam PS, Roy S, Shetty GM. Biomechanical evaluation of a novel S-type, dynamic zero-profile cage design for anterior cervical discectomy and fusion with variations in bone graft shape: a finite element analysis. *World Neurosurg*. 2021;154:e199-e214.
19. Balamurugan S, Chhatoi RK, Dixit V, Manickam PS. Mechanical response of trapezoidal cage on cervical 6–cervical 7 level. *J Eng Sci -med Diagn Ther*. 2023;6:0309071-0309074.
20. Bal BS, Rahaman MN. Orthopedic applications of silicon nitride ceramics. *Acta Biomater*. 2012;8:2889-2898.
21. Pezzotti G, McEntire BJ, Bock R, et al. Silicon nitride: a synthetic mineral for vertebrate biology. *Sci Rep*. 2016;6:31717.
22. Pezzotti G, Marin E, Adachi T, et al. Bioactive silicon nitride: a new therapeutic material for osteoarthropathy. *Sci Rep*. 2017;7:44848.
23. Pezzotti G, McEntire BJ, Bock R, et al. In situ spectroscopic screening of osteosarcoma living cells on stoichiometry-modulated silicon nitride bio ceramic surfaces. *ACS Biomater Sci Eng*. 2016;2:1121-1134.
24. Suh PB, Puttlitz C, Lewis C, Bal BS, McGilvray K. The effect of cervical interbody cage morphology, material composition, and substrate density on cage subsidence. *J Am Acad Orthop Surg*. 2017;25:160-168.
25. McEntire B, Lakshminarayanan R, Ray D, et al. Silicon nitride bearings for total joint arthroplasty. *Lubricants*. 2016;4:35.
26. Pezzotti G. Silicon nitride: a bioceramic with a gift. *ACS Appl Mater Interfaces*. 2019;11:26619-26636.
27. Calvert GC, VanBuren Huffmon G 3rd, Rambo WM Jr, et al. Clinical outcomes for lumbar fusion using silicon nitride versus other biomaterials. *J Spine Surg*. 2020;6:33-48.
28. McEntire BJ, Bal BS, Rahaman MN, Chevalier J, Pezzotti G. Ceramics and ceramic coatings in orthopaedics. *J Eur Ceram Soc*. 2015;35:4327-4369.
29. N M, G R. Effect on lubrication regimes with silicon nitride and bearing steel balls. *Tribol Int*. 2017;116:403-413.
30. Bocanegra-Bernal MH, Matovic B. Mechanical properties of silicon nitride-based ceramics and its use in structural applications at high temperatures. *Mater Sci Eng A*. 2010;527:1314-1338.
31. Olofsson J, Grehk TM, Berlind T, et al. Evaluation of silicon nitride as a wear resistant and resorbable alternative for total hip joint replacement. *Biomatter*. 2012;2:94-102.
32. Mobbs RJ, Rao PJ, Phan K, et al. Anterior lumbar interbody fusion using reaction bonded silicon nitride implants: long-term case series of the first synthetic anterior lumbar interbody fusion spacer implanted in humans. *World Neurosurg*. 2018;120:256-264.
33. Wu TK, Meng Y, Wang BY, et al. Biomechanics following skip-level cervical disc arthroplasty versus skip-level cervical discectomy and fusion: a finite element-based study. *BMC Musculoskelet Disord*. 2019;20:49.
34. Rancourt D, Shirazi-Adl A, Drouin G, Paiement G. Friction properties of the interface between porous-surfaced metals and tibial cancellous bone. *J Biomed Mater Res*. 1990;24:1503-1519.
35. Pooni JS, Hukins DW, Harris PF, Hilton RC, Davies KE. Comparison of the structure of human intervertebral discs in the cervical, thoracic and lumbar regions of the spine. *Surg Radiol Anat*. 1986;8:175-182.
36. Wang J, Qian Z, Ren L. Biomechanical comparison of optimal shapes for the cervical intervertebral fusion cage for C5–C6 cervical fusion using the anterior cervical plate and cage (ACPC) fixation system: a finite element analysis. *Med Sci Monit*. 2019;25:8379-8388.
37. Yoganandan N, Kumaresan S, Pintar FA. Geometric and mechanical properties of human cervical spine ligaments. *J Biomech Eng*. 2000;122:623-629.
38. Zhang QH, Teo EC, Ng HW, Lee VS. Finite element analysis of moment-rotation relationships for human cervical spine. *J Biomech*. 2006;39:189-193.
39. Zhang QH, Teo EC, Ng HW. Development and validation of a CO-C7 FE complex for biomechanical study. *J Biomech Eng*. 2005;127:729-735.
40. Liu S, Li Y, Chen P, et al. Residual stresses and mechanical properties of Si3N4/SiC multilayered composites with different SiC layers. *Bol Soc Esp Ceram Vidr*. 2017;56:147-154.
41. Arab AZE, Merdji A, Benaissa A, et al. Finite-element analysis of a lateral femoro-tibial impact on the total knee arthroplasty. *Comput Methods Programs Biomed*. 2020;192:105446.
42. Manickam PS, Roy S. The biomechanical study of cervical spine: a finite element analysis. *Int J Artif Organs*. 2022;45:89-95.
43. Bhattacharya S, Roy S, Rana M, et al. Biomechanical performance of a modified design of dynamic cervical implant compared to conventional ball and socket design of an artificial intervertebral disc implant: a finite element study. *J Mech Med Biol*. 2019;19:1950017.
44. Biswas JK, Roy S, Pradhan R, Rana M, Majumdar S. Effects of cervical disc replacement and anterior fusion for different bone conditions: a finite element study. *Int J Multiscale Comput Eng*. 2019;17:411-427.
45. Igarashi H, Hoshino M, Omori K, et al. Factors influencing interbody cage subsidence following anterior cervical discectomy and fusion. *Clinical spine surgery*. 2019;32:297-302.
46. Hamada S, Abou-Zeid A. Evaluation of subsidence in stand-alone cervical cage: incidence, risk factors and effects on clinical and radiological picture. *Egypt Spine J*. 2015;14:24-31.
47. Maccormick AP, Sharma H. Analysis of the variables affecting the incidence, location, and severity of cage subsidence following anterior cervical discectomy and fusion operation. *Int J Spine Surg*. 2020;14:896-900.
48. Nakanishi Y, Naito K, Yamagata T, et al. Safety of anterior cervical discectomy and fusion using titanium-coated polyetheretherketone stand-alone cages: Multicenter prospective study of incidence of cage subsidence. *J Clin Neurosci*. 2020;74:47-54.
49. Jin ZY, Teng Y, Wang HZ, et al. Comparative analysis of cage subsidence in anterior cervical decompression and fusion: zero profile anchored spacer (ROI-C) vs. conventional cage and plate construct. *Front Surg*. 2021;8:736680.
50. Lim TH, Kwon H, Jeon CH, et al. Effect of endplate conditions and bone mineral density on the compressive strength of the graft–endplate interface in anterior cervical spine fusion. *Spine*. 2001;26:951-956.
51. Manickam PS, Ghosh G, Shetty GM, Chowdhury AR, Roy S. Biomechanical analysis of the novel S-type dynamic cage by implementation of teaching learning based optimization algorithm-An experimental and finite element study. *Med Eng Phys*. 2023;112:103955.
52. Manickam PS, Ghosh G, Roy S. Optimization of bone graft shapes of S-type cervical cage through genetic algorithm. *Int J Multiscale Comput Eng*. 2022;20:55-79.
53. Sharma A, Kishore H, Singh V, et al. Comparative study of functional outcome of anterior cervical decompression and interbody fusion with tricortical stand-alone iliac crest autograft versus stand-alone polyetheretherketone cage in cervical spondylotic myelopathy. *Glob Spine J*. 2018;8:860-865.
54. Kim YS, Park JY, Moon BJ, Kim SD, Lee JK. Is stand alone PEEK cage the gold standard in multilevel anterior cervical discectomy and fusion (ACDF)? Results of a minimum 1-year follow up. *J Clin Neurosci*. 2018;47:341-346.
55. Ng EP, Yip AS, Wan KH, et al. Stand-alone cervical cages in 2-level anterior interbody fusion in cervical spondylotic myelopathy: results from a minimum 2-year follow-up. *Asian Spine J*. 2019;13:225-231.
56. Barsa P, Suchomel P. Factors affecting sagittal malalignment due to cage subsidence in standalone cage assisted anterior cervical fusion. *Eur Spine J*. 2007;16:1395-1400.
57. Bartels RH, Donk R, van Azn RD. Height of cervical foramina after anterior discectomy and implantation of a carbon fiber cage. *J Neurosurg Spine*. 2001;95:40-42.
58. Yang JJ, Yu CH, Chang BS, et al. Subsidence and nonunion after anterior cervical interbody fusion using a stand-alone polyetheretherketone (PEEK) cage. *Clin Orthop Surg*. 2011;3:16-23.
59. Gei M, Bigoni D, Guicciardi S. Failure of silicon nitride under uniaxial compression at high temperature. *Mech Mater*. 2004;36:335-345.
60. Kulkarni AG, Kumar P, Shetty GM, et al. Finite element analysis comparing the biomechanical parameters in multilevel posterior cervical instrumentation model involving lateral mass screw versus transpedicular screw fixation at the C7 vertebra. *Asian Spine J*. 2024;18:163-170.